Electronic Supplementary Information

Synthesis of a nanogap-rich three-dimensional plasmonic AuNP film for label-free detection of multiple enzymes

Bao-mei Zhou,[a] Rui Song,[a] Juan Hu,*[a] Jinqiu Tao,*[b] Chun-yang Zhang*[a]

[a] School of Chemistry and Chemical Engineering, Southeast University, Nanjing 211189, China.

[b] Division of Breast Surgery, Department of General Surgery, Nanjing Drum Tower Hospital, The Affiliated Hospital of Medical School, Nanjing University, Nanjing 210000, China.

EXPERIMENTAL SECTION

Chemicals and reagents

Chloroauric acid ($HAuCl_4 \cdot 4H_2O$, 99.9%), trisodium citrate ($C_6H_5Na_3O_7 \cdot 2H_2O$, 99%), sodium hydroxide (NaOH) and chloroform ($CHCl_3$, 99.0%) were supplied by Sinopharm Chemical Reagent Co., Ltd. (Shanghai, China). Hydroxylamine hydrochloride ($NH_2OH \cdot HCl$, 98.5%) and R6G ($C_{28}H_{31}N_2O_3Cl$, 97%) were purchased from Shanghai Yuanye Biotechnology Co., Ltd. 4-MBA was purchased from Shanghai Macklin Biochemical Technology Co., Ltd. DTNB was purchased from Shanghai Aladdin Biochemical Technology Co., Ltd. hAAG, UDG, Fpg and recombinant albumin were purchased from New England Biolabs (Ipswich, MA, USA). MMP-2, MMP-9 and MMP-26 were obtained from MedChemExpress (Shanghai, China).

Synthesis of 30-nm, 56-nm, and 66-nm AuNPs

98.9 mL of water and 1 mL of 3% $C_6H_5Na_3O_7 \cdot 2H_2O$ were mixed in a flask, and the mixture was heated to boiling under stirring. Then, 100 μL of 9.8% $HAuCl_4$ was add swiftly to the mixture, followed by boiling for 7 min. The flask was placed in an ice bath to cool for 7 min, and the resulting 16-nm AuNPs were stored as seed solution in a 4 °C refrigerator. Next, 10 mL of 16-nm AuNP seed solution, 9.8 mL of water, 200 μL of 9.8% $NH_2OH \cdot HCl$, and 200 μL of 1% $C_6H_5Na_3O_7 \cdot 2H_2O$ were mixed and stirred for 5 min. Then, 400 μL of 1% $HAuCl_4$ (99.9%) was quickly added to the mixture, followed by stirring at 400 rpm for 1 h. The obtained 22-nm AuNPs were stored in a 4 °C refrigerator. 30-, 56-, and 66-nm AuNPs were prepared by repeating the synthesis steps one, two, and three times, respectively.

Synthesis of 77-nm AuNPs

16-nm AuNP seed solution and 22-nm AuNPs were obtained according to the above method. Subsequently, 4 mL of 22-nm AuNPs, 1.6 mL of 1% $C_6H_5Na_3O_7 \cdot 2H_2O$, 149.6 mL of H_2O, and 1.6 mL of 9.8% $NH_2OH \cdot HCl$ were mixed and stirred for 5 min. Finally, 3.2 mL of 1% $HAuCl_4$ was quickly injected to the mixture, followed by stirring at 400 rpm for 1 h.

Liquid interfacial self-assembly

All glass bottles used in the experiment were immersed in 12 M NaOH for 24 h and then rinsed with water. After the addition of analytes to the AuNPs, the mixture was mixed with chloroform at a volume ratio of AuNPs : chloroform of 3:1. After shaking, AuNPs spontaneously self-assembled to form an assembled SERS substrate with a chloroform-in-water morphology. Correspondingly, a robust assembled SERS substrate with water-in-chloroform morphology was prepared in a container with hydrophobicity.

Electromagnetic field simulation

The electromagnetic field distribution of the proposed AuNP film was investigated by Lumerical Finite-Difference Time-Domain (FDTD). The dielectric constant of AuNP was derived from Au(gold)-Johnson and Christy in FDTD database. The mesh sizes along the x, y, and z directions were all selected as 1 nm. A full-directional PML boundary condition was adopted for the single-particle simulation. Electromagnetic field distribution data were collected by using a two-dimensional DFTM monitor.

Calculation of Raman enhancement factor (EF)

. The Raman *EF* for the 3D plasmonic AuNP film was calculated according to equation S1.[1]

$$EF = \frac{I_{\mathrm{SERS}}}{I_{\mathrm{bulk}}} \frac{N_{bulk}}{N_{\mathrm{SERS}}} \qquad \text{(S1)}$$

where I_{bulk} and I_{SERS} are the signal intensities of DTNB measured by Raman and SERS, respectively. N_{bulk} and N_{SERS} are the amounts of DTNB used in Raman experiment and SERS experiment, respectively.

Contact angle measurements

Contact angle measurements were performed by using a OCA25HTV contact angle goniometer. To ensure statistical reliability, data collection was initiated immediately after the droplet reached the surface of the container.

SERS measurements

Prior to performing SERS detection on the 3D plasmonic AuNP film, the cuvette was soaked in 12 M NaOH for 2 h and then repeatedly rinsed with ultrapure water to render the cuvette hydrophilic. The Raman spectra were obtained from a XploRA PLUS (HORIBA) with a 785-nm laser.

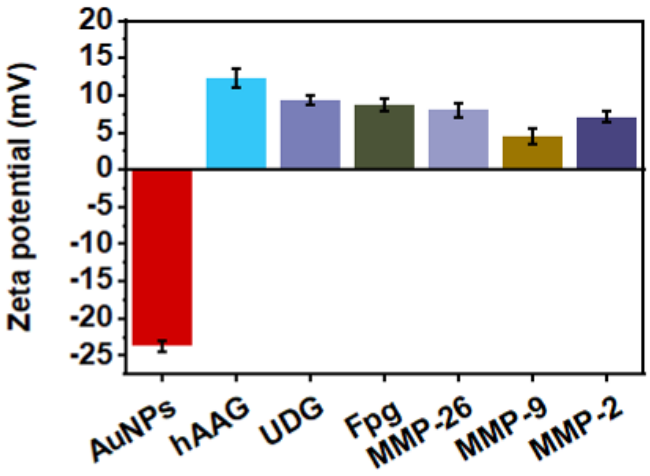

Fig. S1 Zeta potential analysis of the AuNPs, hAAG, UDG, Fpg, MMP-26, MMP-9, and MMP-2.

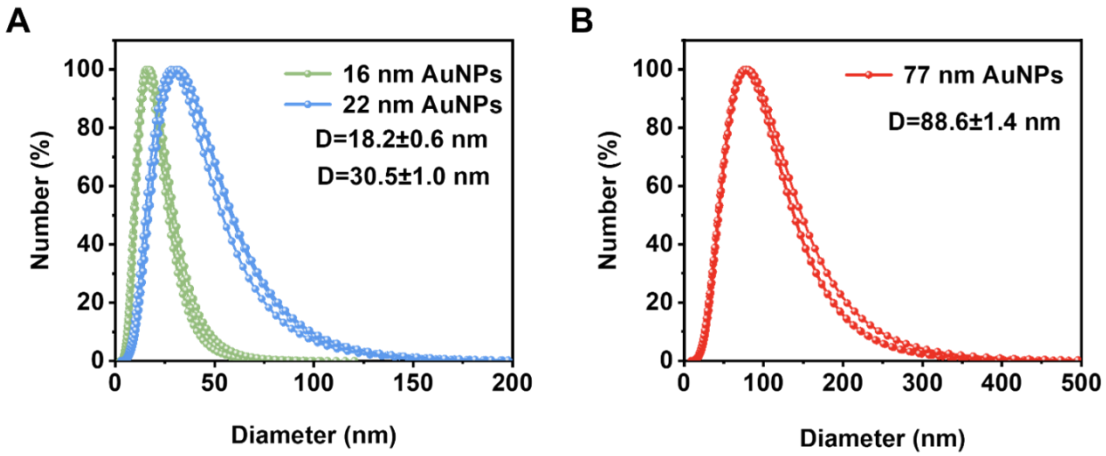

Fig. S2 (A) Hydrodynamic size distribution of the 16-nm and 22-nm AuNPs. (B) Hydrodynamic size distribution of the 77-nm AuNPs.

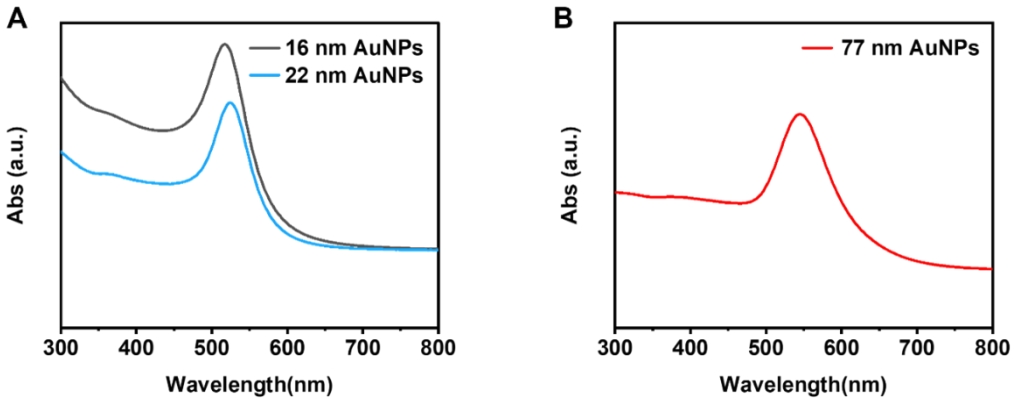

Fig. S3 (A) UV-Vis absorbance spectra of 16-nm and 22-nm AuNPs. (B) UV-Vis absorbance spectra of 77-nm AuNPs.

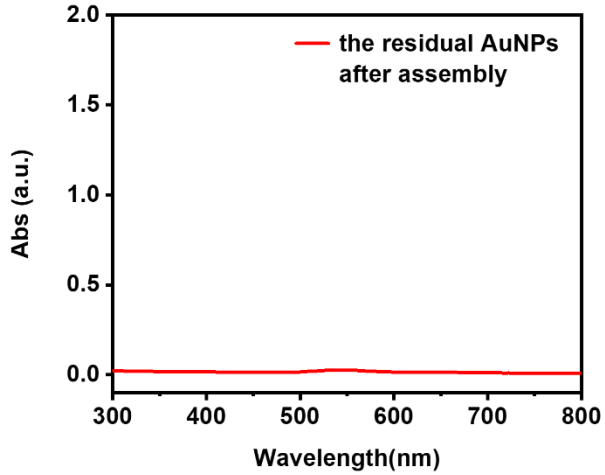

Fig. S4 UV-vis measurement of the residual AuNPs in the supernatant after the assembly of 3D plasmonic AuNP film.

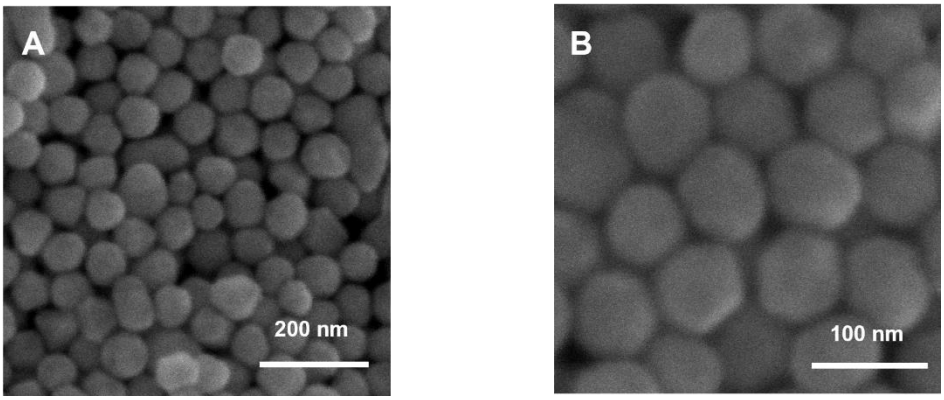

Fig. S5 (A) SEM images of the3D plasmonic AuNP film prepared with 77-nm AuNPs and the enlarged SEM image (B).

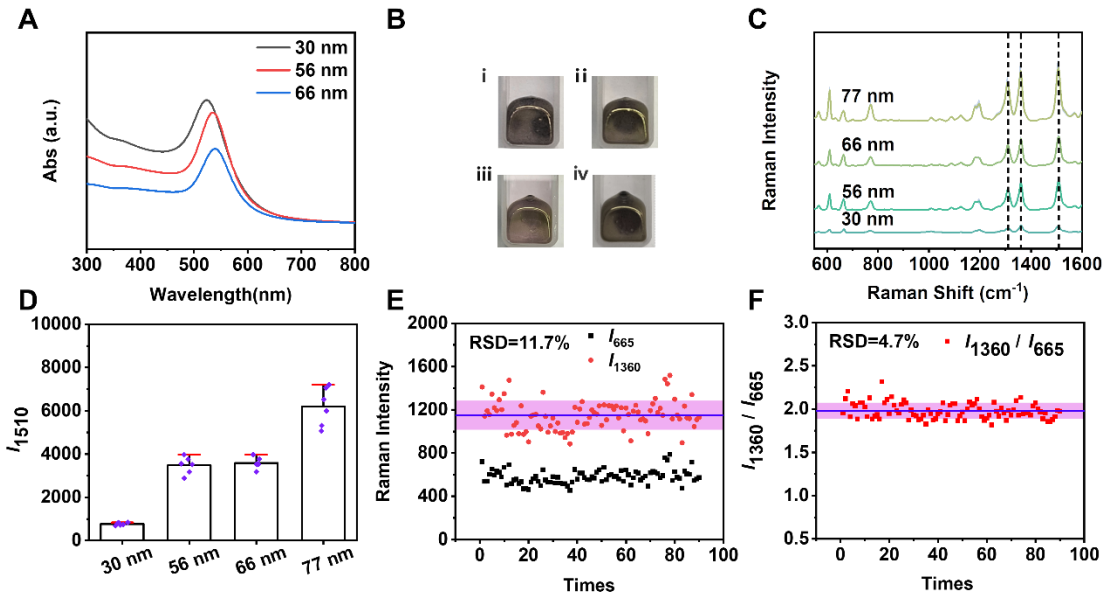

Fig. S6 (A) UV-Vis absorbance spectra of 30-nm, 56-nm, and 66-nm AuNPs. (B) Optical images of nanoparticle film composed of 30-nm AuNPs (i), 56-nm AuNPs (ii), 66-nm AuNPs (iii), and 77-nm AuNPs (iv). (C) R6G SERS spectra generated from 3D plasmonic AuNP films composed of different sizes of AuNPs. (D) Statistical analysis of the peak intensities at 1510 cm^{-1} for spectra in (C). Error bar denotes mean ± SD (n = 6). (E) RSD of SERS intensities at 1510 cm^{-1} obtained from 90 spectra recorded on the 3D plasmonic AuNP films. (F) RSD of the intensity ratio (I_{1510} / I_{665}) calculated from the same set of spectra.

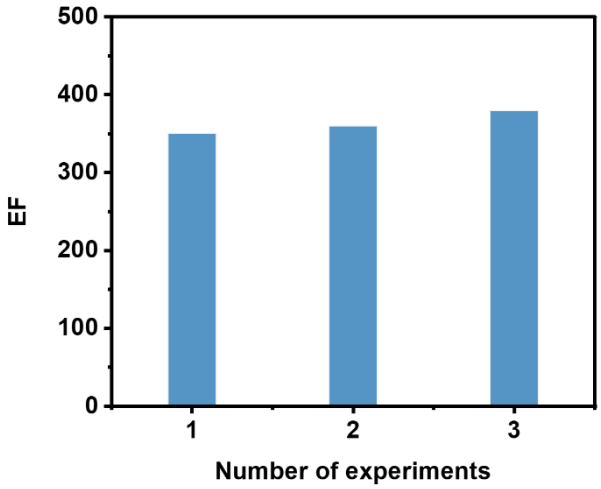

Fig. S7 Raman enhancement factor (EF) of gold sols in response to DTNB molecule with the amount of 6.02×10^{16}.

Assessment the versatility of SERS platform

To assess the versatility of this 3D plasmonic AuNP film-based SERS platform, UDG, Fpg, MMP-9, MMP-2, 4-MBA, and DTNB were analyzed. UDG and Fpg are DNA glycosylases that can disturb DNA damage repair process. MMP-9 and MMP-2 are matrix metalloproteinases can degrade multiple components of extracellular matrix (ECM). 4-MBA (pH-sensitive Raman reporters) and DTNB (protein disulfide isomerase inhibitor) are selected as the small molecule targets. UDG possesses the distinctive SERS peaks at 515 cm^{-1} (S-S), 730 cm^{-1} (C-S), 818 cm^{-1} (serine), 890 cm^{-1} (tryptophan), 1164 cm^{-1} (tyrosine or phenylalanine), 1230 cm^{-1} (amide III), and 1565 cm^{-1} (amide II) (Fig. S7A). Fpg possesses the distinctive SERS peak at 1620 cm^{-1} (amide I) (Fig. S7B). [2-4] We measured the Raman intensity at 1565 cm^{-1} and 1620 cm^{-1} induced by various-concentration UDG and Fpg, respectively. Raman intensity at 1565 cm^{-1} and 1620 cm^{-1} enhance with the increasing concentrations of UDG and Fpg, respectively (Figs. S7C,E). The regression equations are $Y = 0.62 \log_{10} C + 1.95$ ($R^2 = 0.992$) for UDG assay and $Y = 20.70 \log_{10} C + 0.16$ ($R^2 = 0.999$) for Fpg assay,

where Y represents the intensity ratio (I_{1565} / I_{665} for UDG, I_{1630} / I_{665} for Fpg) and C represents the enzyme concentrations (Figs. S7D,F). The LOD is estimated to be 0.00125 U/μL for UDG and 0.001 U/μL for Fpg. MMP-26 possesses the distinctive peaks of 1505 cm^{-1} (histidine) and 1608 cm^{-1} (tyrosine and/or phenylalanine). MMP-9 possesses characteristic peak of 911 cm^{-1} ($-COO^-$). MMP-2 possesses characteristic peak of 1614 cm^{-1} (tyrosine). Specifically, MMP-26 and MMP-9 demonstrate common peaks at 593 cm^{-1} (tryptophan). MMP-26, MMP-9 and MMP-2 show common peaks at 732 cm^{-1} (C-S), 860 cm^{-1} (tyrosine), 1010 cm^{-1} (phenylalanine), 1128 cm^{-1} (chromophore protein $\nu_{14}B_{1g}$ and/or phenylalanine), 1238 cm^{-1} (C-N stretching and/or amide III), 1392 cm^{-1} (ν_s (COO-)), and 1444 cm^{-1} (CH_2 scissor).[2, 4-9]

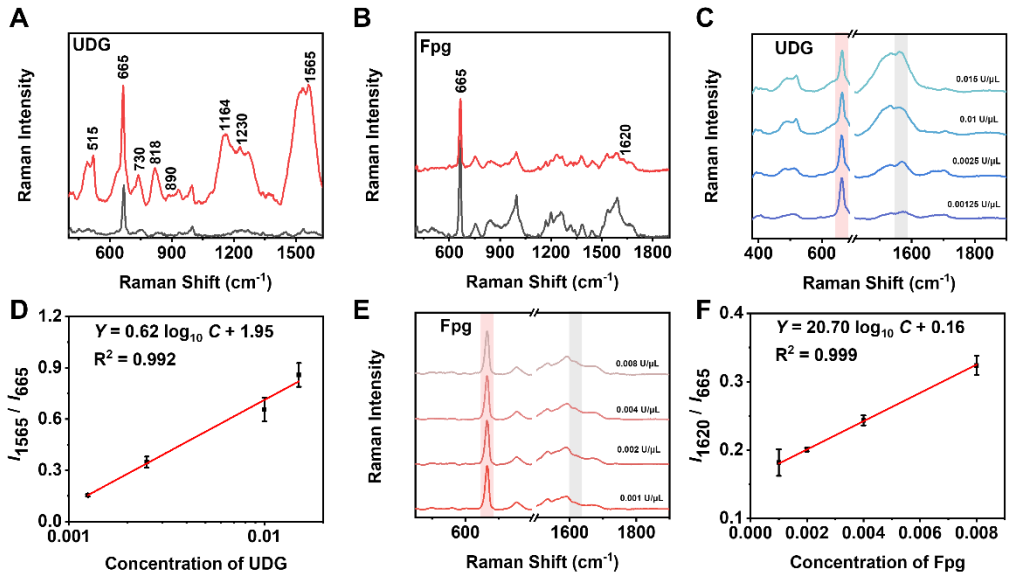

Fig. S8 (A) SERS spectra acquired from the 3D plasmonic AuNP film in the presence (red line) and absence (black line) of UDG. (B) SERS spectra acquired from the 3D plasmonic AuNP film in the presence (red line) and absence (black line) of Fpg. (C) SERS spectra of UDG at different concentrations. (D) Linear correlation of the I_{1565} / I_{665} SERS intensity ratio with the UDG concentration. (E) SERS spectra of Fpg at different concentrations. (F) Linear correlation of the I_{1620} / I_{665} SERS intensity ratio with the Fpg concentration. Error bar denotes mean ± SD (n = 3).

4-MBA shows distinctive peaks at 1074 cm^{-1} and 1584 cm^{-1}, and SERS intensity of these two peaks enhances with the increasing concentration of 4-MBA (Fig. S8A). An excellent Langmuir fitting with R^2 = 0.994 is plotted between I_{1074} / I_{665} and 4-MBA concentrations (Fig. S8D). The LOD is estimated to be 10^{-12} M. The sensitivity of this platform is much higher than those of previously reported methods for 4-MBA assay, with 3 orders of magnitude higher than that of Ag- and Au-coated silicon filter substrate-based SERS assay.[10] DTNB shows peaks at 1337 cm^{-1} and 1558 cm^{-1}, and their intensity enhances with the increasing concentration of DTNB (Fig. S8B). An excellent Langmuir fitting with R^2 = 0.933 is plotted between I_{1337} / I_{665} and DTNB concentrations (Fig. S8E). The LOD is estimated to be 10^{-13} M. The sensitivity of this platform is much higher than those of reported methods for DTNB assay, with 8 orders of magnitude higher than that of metal layers substrate-based SERS assay,[11] 3 orders of magnitude higher than that of magnetic polyphosphazene-Ag composite particles-based SERS assay.[12]

To assess the multiplexing capability of SERS platform for small molecule detection, we simultaneously measured 4-MBA and DTNB (Fig. S8C). The characteristic peaks at 1074 cm^{-1} and 1584 cm^{-1} (4-MBA), and 1337 cm^{-1}, 1558 cm^{-1} (DTNB) are clearly observed in the mixture spectra, suggesting that this SERS platform enables simultaneously and accurately identify multiple small molecules in a single assay.

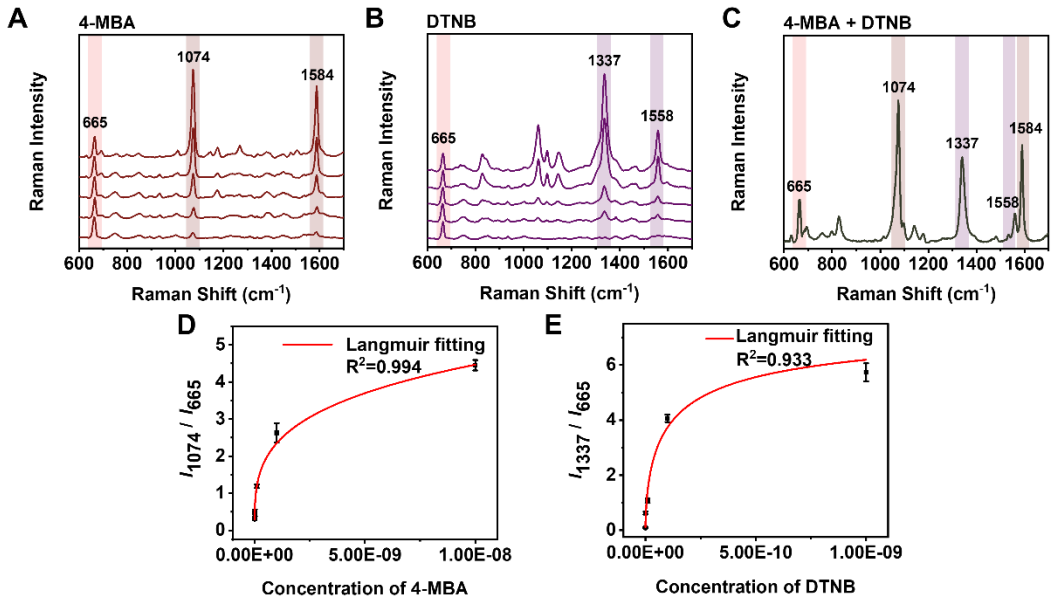

Fig. S9 (A) SERS spectra of different-concentration 4-MBA. (B) SERS spectra of different-concentration DTNB. (C) SERS spectra in the presence of 4-MBA + DTNB. (D) Relationships between the I_{1074} / I_{665} SERS intensity ratio and the 4-MBA concentration. (E) Relationships between the I_{1337} / I_{665} SERS intensity ratio and the DTNB concentration. Error bar denotes mean ± SD (n = 3).

Table S1. Peaks assignments for the SERS spectra of hAAG, UDG and Fpg

Raman Shift	Assignment	References
603	hAAG, Phe	5
718	hAAG, Pro	5, 6
858	hAAG, Tyr, Phe, Pro	6
1006	hAAG, Phe	2
1130	hAAG, $\nu_{14}B_{1g}$, Phe	2
1238	hAAG, Amide III, Trp	2, 5
1380	hAAG, ν (COO-)	2, 5
1453	hAAG, Tyr	13
515	UDG, S-S	2
730	UDG, C-S (protein)	6
818	UDG, Ser (γ: COOH-)	3
890	UDG, Trp	5
1164	UDG, Tyr, Phe	5
1230	UDG, Amide III	2, 6
1565	UDG, Amide II	4
1620	Fpg, Amide I	4

Table S2. Peaks assignments for the SERS spectra of MMP-26, MMP-9 and MMP-2

Raman Shift (cm^{-1})	Assignment	References
593	MMP-26, MMP-9, Trp	7
704	MMP-26; MMP-9, MMP-2, /	/
732	MMP-26, MMP-9, MMP-2, C-S (protein)	6
860	MMP-26, MMP-9, MMP-2, Tyr	5
1010	MMP-26, MMP-9, MMP-2, Phe	5
1128	MMP-26, MMP-9, MMP-2, chromophore protein $\nu_{14}B_{1g}$,	2
1238	MMP-26, MMP-9, MMP-2, C-N stretching, Amide III	2, 6, 8
1392	MMP-26, MMP-9, MMP-2, ν_s(COO-)	2
1444	MMP-26, MMP-9, MMP-2, CH_2 scissor	5, 9
1505	MMP-26, His	7
1608	MMP-26, Tyr and/or Phe	5
911	MMP-9, $-COO^-$	4
1614	MMP-2, Tyr, in-ring CC stretch	5, 8

Table S3. Peaks assignment for the SERS spectra of 4-MBA and DTNB

Raman Shift (cm^{-1})	Assignment	References
1074	4-MBA, C-S stretching vibration	14, 15
1584	4-MBA, breathing mode of aromatic ring	14, 15
1337	DTNB, the asymmetric NO_2	14, 16
1558	DTNB, aromatic ring vibration	14, 16

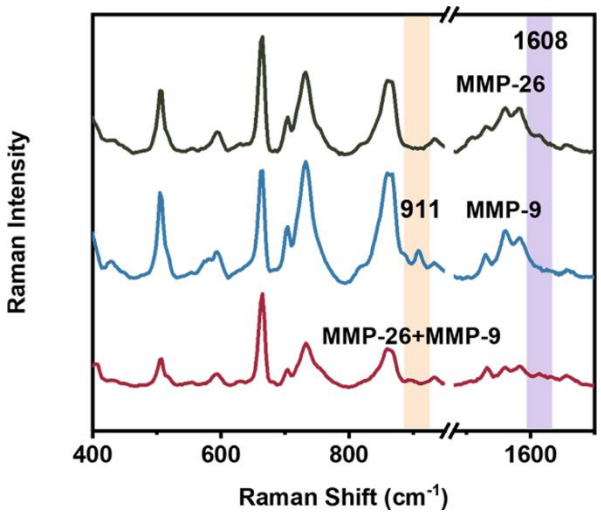

Fig. S10 Comparison of SERS spectra after treatment with MMP-26 (1608 cm^{-1}), MMP-9 (911 cm^{-1}), and MMP-26 + MMP-9.

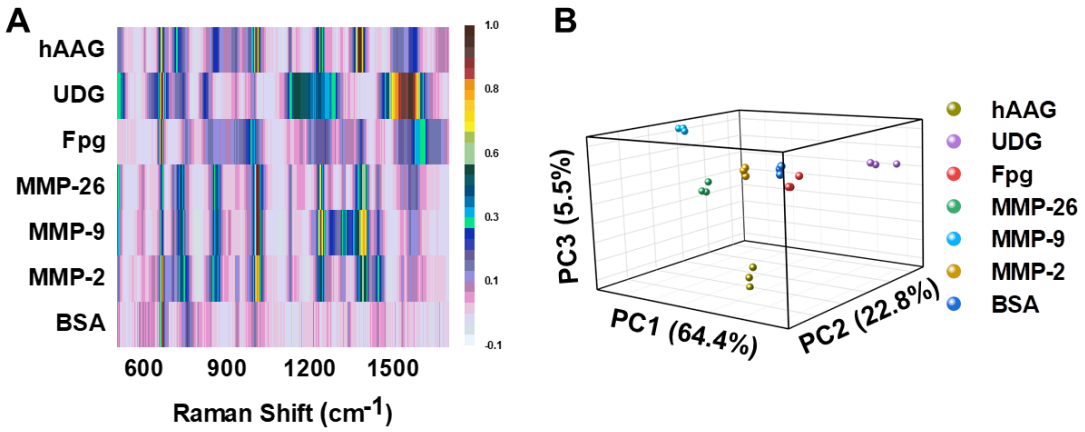

Fig. S11 (A) Heat map of SERS intensities of seven proteins. (B) PCA score plot of the SERS data of seven proteins.

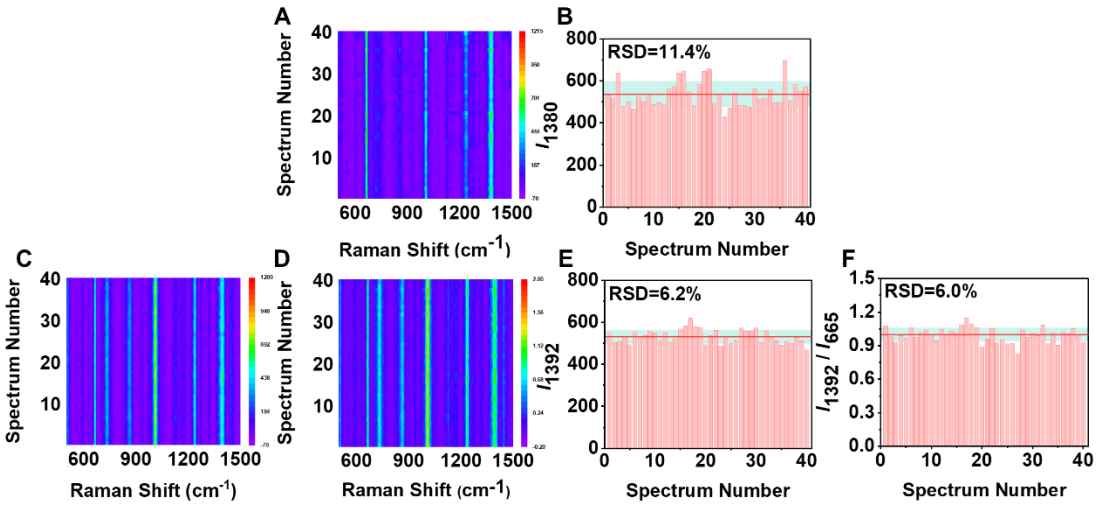

Fig. S12 (A) 2D SERS spectral mapping generated from a set of 40 hAAG spectra before calibration. (B) Histogram of SERS intensities at 1380 cm^{-1} for 40 spectra in (A). 2D SERS spectral mapping generated from a set of 40 MMP-26 spectra before (C) and after (D) calibration. (E) Histogram of SERS intensities at 1392 cm^{-1} for 40 spectra in (C). (F) Histogram of the intensity ratio of I_{1392} / I_{665} for 40 spectra in (D).

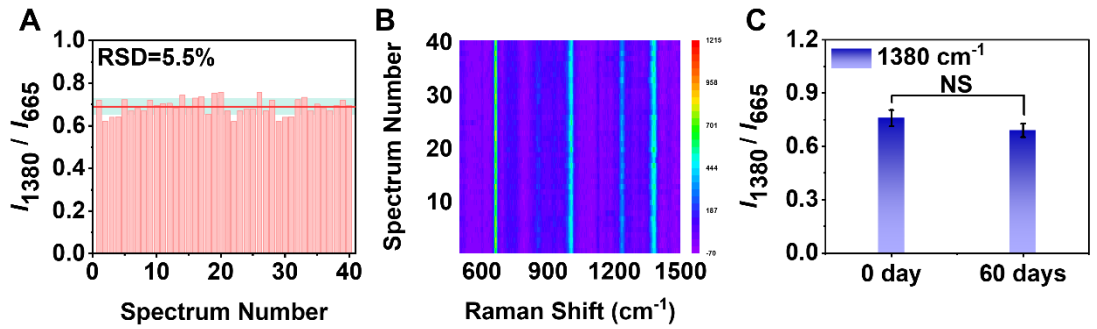

Fig. S13 (A) Histogram of the intensity ratio of I_{1380} / I_{665} for 40 hAAG spectra. The spectra are collected randomly from the plasmonic AuNP film stored for 60 days. (B) 2D SERS spectral mapping generated from 40 hAAG spectra before calibration by chloroform. The spectra are collected randomly from the plasmonic AuNP film stored for 60 days. (C) Measurement of the intensity ratio of I_{1380} / I_{665} recorded at 0 and 60 days by the plasmonic film.

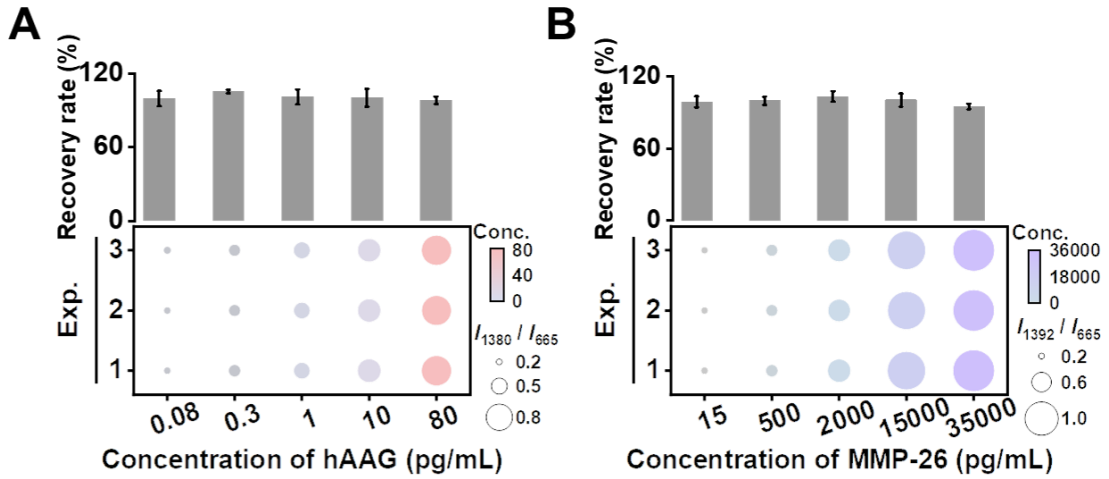

Fig. S14 (A) Recovery ratios (top) and heat map (bottom) of hAAG analysis in serum samples. (B) Recovery ratios (top) and heat map (bottom) of MMP-26 analysis in serum samples.

Table S4. Detection of hAAG level in fetal bovine serum

Sample	Added (pg/mL)	Measured (pg/mL)	RSD (%)
1	0.08	0.084	6.16
2	0.3	0.33	1.63
3	1	1.27	5.88
4	10	10.53	7.47
5	80	82.47	3.18

Table S5. Detection of MMP-26 level in fetal bovine serum

Sample	Added (pg/mL)	Measured (pg/mL)	RSD (%)
1	15	14.80	4.60
2	500	497.94	3.52
3	2000	2063.46	4.23
4	15000	15034.92	5.52
5	35000	33196.04	2.45

Table S6. Comparison of the proposed 3D plasmonic AuNP film with other reported SERS substrates

SERS substrates	Raman enhancement factor	Ref.
silver nanosheet	1.01×10^5	17
SiO_2@AuAg	1.22×10^5	18
Ag−Cu_2O hybrids	1.4×10^5	19
Co/C@Ag/g-C_3N_4	1.3×10^6	20
TiO_2 superstructures	2.64×10^5	21
three-dimensional plasmonic AuNP film	5.9×10^6	Our work

REFERENCES

1. L. Zhang, W. C. Yi, J. F. Li, G. Y. Wei, G. C. Xi and L. Q. Mao, *Nat. Commun.*, 2023, **14**, 6318.
2. D. Li, Z. Zhang, X. T. Wang, Y. P. Wang, X. Gao and Y. Li, *Biosens. Bioelectron.*, 2022, **200**, 113907.
3. T. Gao, T. Yachi, X. Shi, R. Sato, C. Sato, Y. Yonamine, K. Kanie, H. Misawa, K. Ijiro and H. Mitomo, *ACS Nano*, 2024, **18**, 21593-21606.
4. A. Sánchez-Illana, F. Mayr, D. Cuesta-García, J. D. Piñeiro-Ramos, A. Cantarero, M. de la Guardia, M. Vento, B. Lendl, G. Quintás and J. Kuligowski, *Anal. Chem.*, 2018, **90**, 9093-9100.
5. M. Chen, H. Y. Wang, Y. B. Zhang, H. Y. Jiang, T. Li, L. X. Liu and Y. T. Zhao, *Anal. Chem.*, 2024, **96**, 6794-6801.
6. G. H. Qi, X. K. Diao, S. P. Hou, J. Kong and Y. D. Jin, *Anal. Chem.*, 2022, **94**, 14931-14937.

7. E. Podstawka, Y. Ozaki and L. M. Proniewicz, *Appl. Spectrosc.*, 2004, **58**, 1147-1156.
8. Y. F. Jiang, S. S. Du, M. Xu, T. Yu, B. M. Zhou, F. F. Yu, H. Jiang, L. A. Yang, M. K. Su and H. L. Liu, *Food Chem.*, 2022, **382**, 132237.
9. G. Y. Zhu, X. Zhu, Q. Fan and X. L. Wan, *Spectrochim. Acta. A. Mol. Biomol. Spectrosc.,* 2011, **78**, 1187-1195.
10. L. Mikac, H. Gebavi, J. Perrault and M. Ivanda, *Spectrochim. Acta. A. Mol. Biomol. Spectrosc.*, 2025, **339**, 126255.
11. M. K. Ulku, A. Gumustas, U. Tamer, M. A. S. Arikan and E. Yildirim, *J. Raman Spectrosc.*, 2025, **56**, 1469-1478.
12. C. Huang, F. F. Lu, K. Xu, G. J. Ding, L. J. You, J. B. Wang and Q. Q. Zhang, *Chin. Chem. Lett.*, 2019, **30**, 2009-2012.
13. F. Madzharova, Z. Heiner and J. Kneipp, *J. Phys. Chem. C*, 2017, **121**, 1235-1242.
14. J. Tu, T. Wu, Q. Yu, J. X. Li, S. Zheng, K. Z. Qi, G. H. Sun, R. Xiao and C. W. Wang, *J. Hazard. Mater.,* 2023, **448**. 130912.
15. R. Y. Liu, L. Jiang, Z. Z. Yu, X. F. Jing, X. Liang, D. Wang, B. Yang, C. X. Lu, W. Zhou and S. Z. Jin, *Sens. Actuators B Chem.,* 2021, **333**, 129581.
16. C. Duffield, N. Lyu and Y. L. Wang, *J. Innov. Opt. Health Sci.* 2021, **14**, 2141007.
17. T. Zhang, Y. T. Li, X. M. Lv, S. Jiang, S. Jiang, Z. Q. Sun, M. X. Zhang and Y. Li, *Adv. Funct. Mater.*, 2024, **34**, e202315668.
18. R. Z. Zhang, S. B. Xie, X. Y. Yang, Y. Liu, X. J. Luo and Y. He, *Biosens. Bioelectron.*, 2025, **288**, 117777.
19. M. Zhou, X. F. He, L. Y. Niu, C. Li, T. Q. Chen and Y. Y. Gong, *J. Alloys Compd.*, 2024, **971**,

172476.

20. G. T. Chen, F. Mi, S. Zhang, X. H. Rao, J. Sun, Z. Yang and M. Guan, *Food Chem.*, 2025, **493**, 145723.

21. J. J. Zhao, L. Sun, Y. M. Dong, Y. X. Chang, H. S. Wang, Z. H. Liu, J. B. Li, Y. F. Xie and W. Ji, *Nano Lett.*, 2025, **25**, 6645-6653.